

ARTICLE OPEN



Symmetry of magnetic correlations in spin-triplet superconductor UTe_2

Nicholas P. Butch ^{1,2}✉, Sheng Ran ^{1,2,3}, Shanta R. Saha^{1,2}, Paul M. Neves^{1,2}, Mark P. Zic^{1,2}, Johnpierre Paglione ^{1,2}, Sergiy Gladchenko¹, Qiang Ye^{1,4} and Jose A. Rodriguez-Rivera ^{1,4}

The temperature dependence of the low-energy magnetic excitations in the spin-triplet superconductor UTe_2 was measured via inelastic neutron scattering in the normal and superconducting states. These excitations have a peak intensity at 4 meV, follow the Brillouin zone edges near the crystallographic b-axis, obey the paramagnetic structural symmetry, and track the temperature evolution of the heavy fermion bulk magnetic susceptibility. Thus, the imaginary part of the dynamic susceptibility follows the behavior of interband correlations in a hybridized Kondo lattice with an appropriate characteristic energy. These excitations are a lower-dimensional analog of phenomena observed in other Kondo lattice materials, such that their presence is not necessarily due to dominance of ferromagnetic or antiferromagnetic correlations. The onset of superconductivity alters the magnetic excitations noticeably on the same energy scales, suggesting that these changes originate from additional electronic structure modification.

npj Quantum Materials (2022)7:39; <https://doi.org/10.1038/s41535-022-00445-7>

INTRODUCTION

Spin-triplet superconductivity was recently discovered in UTe_2 ¹. The superconductivity is characterized by large and anisotropic upper critical fields that all exceed the paramagnetic limit, pointing to unconventional spin-triplet pairing^{1,2}. Superconductivity is limited by a magnetic phase transition at 35 T^{3,4}, and the field-polarized state contains another reentrant superconducting phase above 40 T³. Superconductivity in UTe_2 is believed to be topologically nontrivial because of observations of chiral in-gap surface states⁵, a double transition in specific heat, and broken time reversal symmetry as detected by optical Kerr rotation⁶, which suggest the presence of a complex, two-component superconducting order parameter. Consistent with a p-wave orbital symmetry, the superconducting gap is nodal^{7–9}.

Superconductivity emerges from a renormalized electronic structure of hybridized f-electrons. UTe_2 exhibits archetypal heavy fermion features, namely a large low-temperature specific heat and local maxima in temperature-dependent electrical resistivity and magnetic susceptibility below room temperature¹, a Kondo hybridization gap of 4 meV in scanning tunneling spectroscopy⁵, quadratic temperature dependence of low-temperature resistivity¹⁰, linear temperature dependence of thermoelectric power¹¹, and a Drude peak in optical conductivity¹². Angle resolved photoemission (ARPES) measurements show that the band structure of UTe_2 is dominated by two intersecting one-dimensional sheets¹³. The heavy electron states result from hybridization between these highly-dispersive bands with f-electron states near the chemical potential, as suggested by dynamical mean field theory (DMFT) calculations^{12,13}, while ARPES also reveals an additional Fermi pocket that is three-dimensional and potentially heavy.

Magnetic interactions play an important role in UTe_2 . Low-temperature neutron diffraction demonstrates the lack of long range magnetic order in the normal state¹⁴. Yet several measurements suggest proximity to a ferromagnetic instability.

A scaling analysis of the magnetization suggests the influence of ferromagnetic quantum critical fluctuations¹. Muon spin relaxation measurements have shown that significant spin fluctuations in the normal state strengthen upon cooling into the superconducting state¹⁵. Nuclear magnetic resonance measurements are difficult at low temperature in the normal state due to long relaxation times¹⁶. Optical Kerr rotation experiments reveal that vortices consist of magnetically polarizable normal cores¹⁷.

Recent inelastic neutron scattering experiments complicate the picture, as they have not found obvious signatures of ferromagnetic fluctuations, but rather magnetic excitations at incommensurate wavevectors. These might originate in RKKY interactions or Fermi surface nesting¹⁸, or rod-like excitations due to spin-ladder interactions¹⁹. Intriguingly, a change in the inelastic neutron scattering emerges in the superconducting state, near energies of 1 meV^{20,21}, which is suggested to be a type of superconducting resonance. Recent calculations show that a dominant antiferromagnetic susceptibility can be consistent with spin-triplet superconductivity²².

We performed a series of inelastic neutron scattering experiments in the crystallographic a-b plane that demonstrate the detailed energy-dependence and anisotropy of the magnetic excitations. The excitations evolve over a broad range of temperatures, from the weakly correlated high-temperature state into the superconducting state below 1.6 K. These excitations are signatures of the heavy electron band structure, similar to several other Kondo lattice systems, but with a lower dimensionality due to the UTe_2 structure. They do not a priori imply a tendency toward a specific type of long-range magnetic order. These measurements also show that the change in the excitation spectrum in the superconducting state is a phenomenon that occurs over energies of several meV, suggesting a substantial change in magnetic correlations at low temperatures.

¹NIST Center for Neutron Research, National Institute of Standards and Technology, Gaithersburg, MD 20899, USA. ²Maryland Quantum Materials Center, Department of Physics, University of Maryland, College Park, MD 20742, USA. ³Department of Physics, Washington University in St. Louis, St. Louis, MO 63130, USA. ⁴Department of Materials Science and Engineering, University of Maryland, College Park, MD 20742-2115, USA. ✉email: nbutch@umd.edu

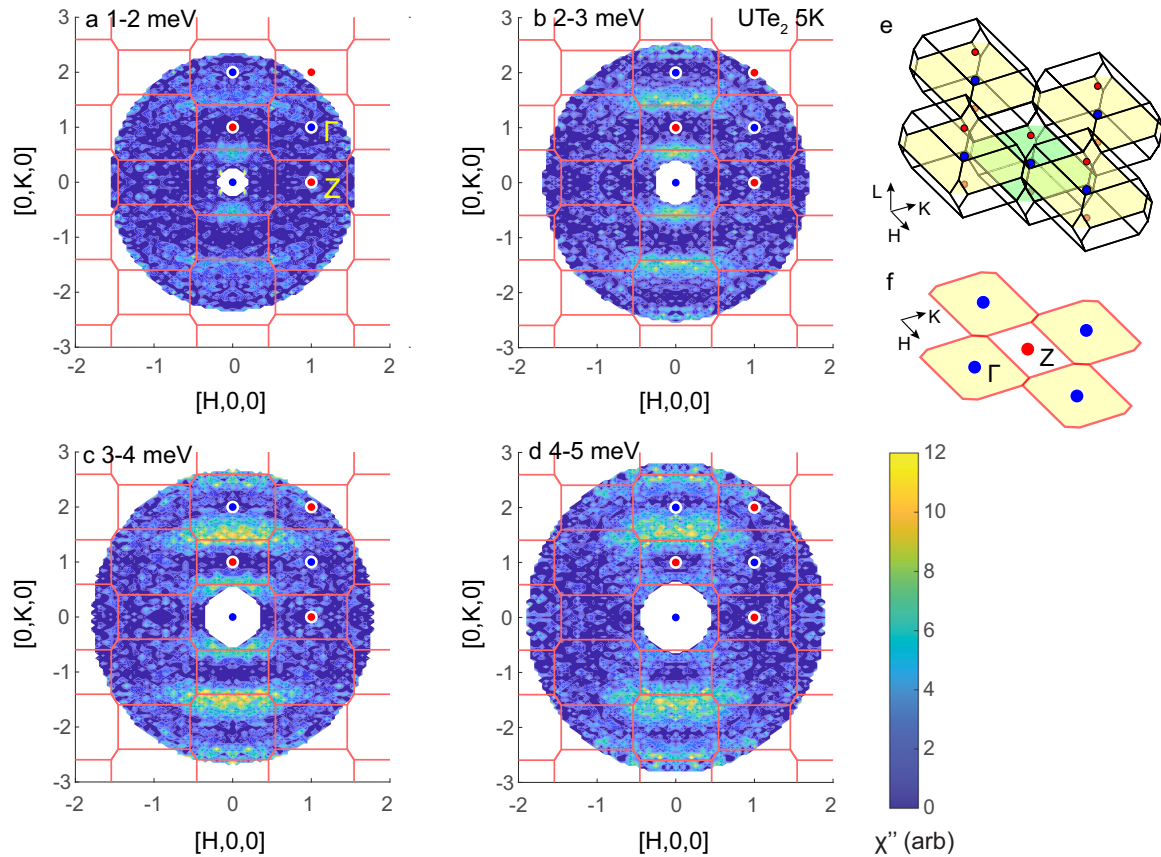


Fig. 1 Imaginary part of the dynamic magnetic susceptibility $\chi''(Q, E)$ of UTe_2 at 5 K, in the regime of strong hybridization, as measured by neutron scattering. The susceptibility in the $[H, K, 0]$ plane, corresponding to the crystallographic (a, b) plane is strongest in the energy intervals (a) 1–2 meV, (b) 2–3 meV, (c) 3–4 meV, (d) 4–5 meV. These inelastic magnetic excitations closely follow the Brillouin zone edges (red) along the K direction. These excitations do not extend much beyond $H=0.5$ and are absent in symmetrically equivalent Brillouin zones that are not centered on $H=0$. Blue and red circles mark the Brillouin zone centers Γ and Brillouin zone faces Z , respectively, which are neighbors in the $[H, K, 0]$ plane due to the body-centered crystal structure, shown in (e) three and (f) two dimensions.

RESULTS AND DISCUSSION

Inelastic neutron scattering

The scattered neutron intensity S , measured as a function of transfer of momentum Q and energy E , is proportional to a temperature factor times the imaginary part of the dynamic magnetic susceptibility χ'' , by $\chi''(Q, E) = (1 - e^{-\beta E})S(Q, E)$, where k_B is the Boltzmann constant and T is the temperature. In UTe_2 , the dominant feature in χ'' has a well-defined Q -dependence with peak intensity at $E=4$ meV. As shown in Fig. 1, at 5 K these magnetic excitations essentially form stripes long in the H direction, the crystallographic a -axis, and modulated along the K direction, the b -axis. The body-centered orthorhombic crystal structure of UTe_2 is in the space group $Immm$ with lattice constants $a=4.12$ Å, $b=6.08$ Å, and $c=13.8$ Å at 2.7 K¹⁴. The $Immm$ primitive lattice vectors are along the body diagonals of the conventional orthorhombic cell and the Brillouin zone (BZ) is not a rectangular prism. Nearest-neighbor BZ's along the H and K directions are displaced in the L direction, resulting in a pattern of alternating centers and faces in the $[H, K, 0]$ plane.

As the BZ overlays in Fig. 1 make clear, the magnetic excitations are confined to the edges of the BZ's, occurring at values of $K = 0.6 = \frac{1}{2}(1 + \frac{b^2}{a^2})$ and symmetrically equivalent values such as $K = 1.4$ and $K = 2.6$. However, the excitations are constrained to near $H=0$ and are not detected at the edges of any BZ's that do not fall on the K axis, even though these would be expected because they are symmetrically equivalent. Weak excitations at larger H values²⁰ are not evident here. There is disagreement over whether similar excitations extend along the L direction^{18,19}. It is interesting

that the intensity distribution along the BZ edge shows some dependence on K at low E (Fig. 1): it is stronger in the middle at $K=0.6$ and distributed towards the corners at $K=1.4$. This intensity variation cannot be explained by a standard uranium 5f-electron form factor, which would monotonically decrease the intensity at higher Q , or simple spin polarization²³, suggesting a more complicated origin. The majority of the spectral weight sits at higher energies, and a further comparison above 3 meV of the $K=0.6$ and $K=1.4$ excitations is not possible because of the kinematic scattering limits of the spectrometer.

Looking more closely at the Q -dependence, it is clear that the excitations disperse asymmetrically. Figure 2 shows contour plots of χ'' at 5 K, comparing the magnetic dispersion along (a) the b -axis and (b) the a -axis at the BZ edge. To more easily see the Q -dependence in the vicinity of $[0, 1.4, 0]$, these data are broken up into constant- Q scans in Fig. 2c. Fits of Lorentzian lineshapes can describe the data adequately. The energy of peak intensity can be tracked as a function of Q (Fig. 2d). There is an obvious, sharp minimum in the peak position at $K=1.4$ with a value of 4 meV, which remains approximately constant as a function of H along $[H, 1.4, 0]$. Thus the excitation is not dispersive along the BZ edge, but only along the perpendicular direction. Note also that the dispersion along $[0, K, 0]$ is very asymmetric about the minimum at $K=1.4$, with a steeper slope of -16 meV Å at smaller K and shallower slope of 5.5 meV Å at larger K . This follows the asymmetry of the paramagnetic body-centered unit cell - note that the excitations for $K < 1.4$ actually extend along a BZ face, while for $K > 1.4$ they are inside the volume of the BZ as they

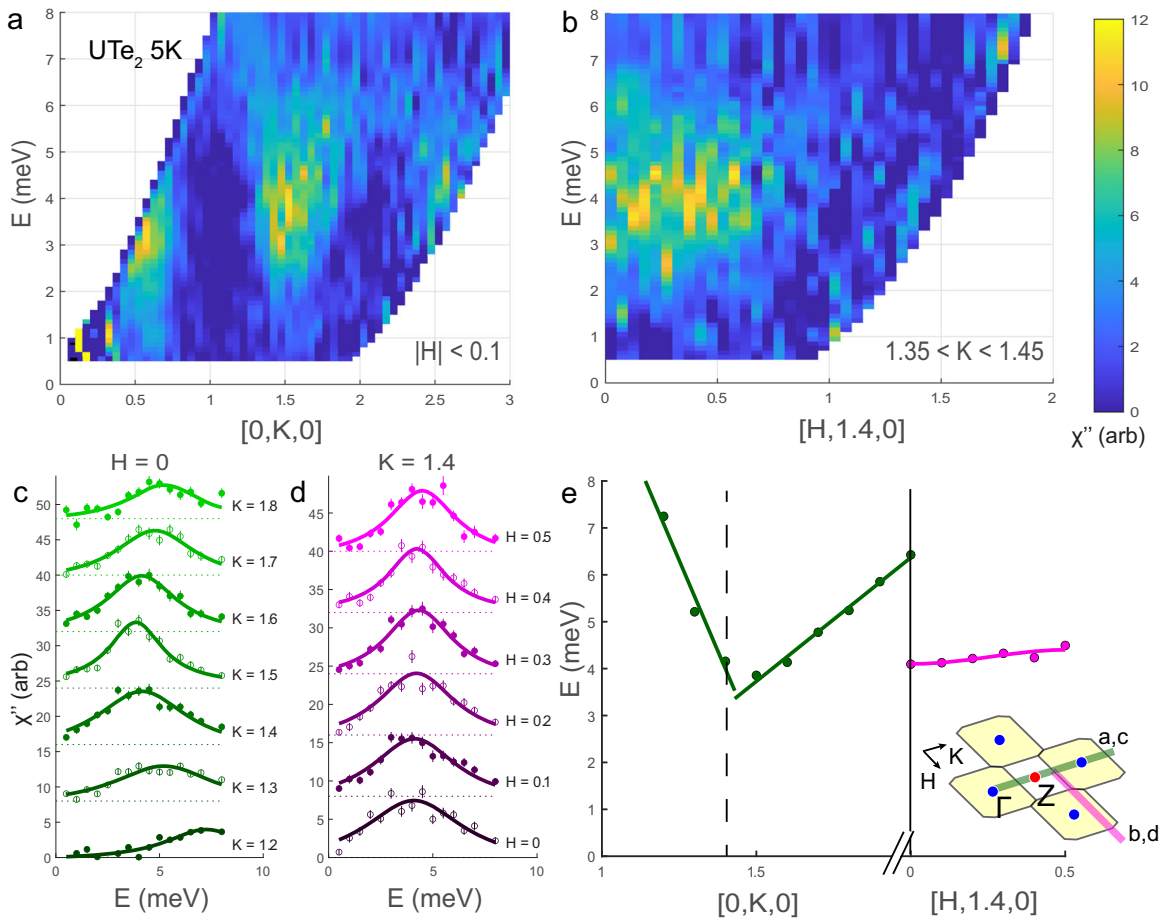


Fig. 2 The anisotropic Q -dependence of the magnetic susceptibility $\chi''(Q, E)$ in UTe_2 at 5 K along different slices of the $[H, K, 0]$ plane. **a** $\chi''(Q, E)$ as a function of K at constant $H = 0$. Along this direction, the dispersion is V-shaped and sharp, with energy minima at $K = 0.6, 1.4$ and 2.6 , corresponding to the Brillouin zone boundaries. **b** $\chi''(Q, E)$ as a function of H at constant $K = 1.4$. The susceptibility is flat in the H direction, extending to $H = 0.5$, the edge of the Brillouin zone. **c**, **d** Effective constant- Q scans show the E -dependence of χ'' at selected values of K from **(a)** and H from **(b)**. Curves are fits to Lorentzian lineshapes, which show that the width of the magnetic excitations is of order the peak energy. Whereas the lineshapes are rather dependent of K , there is relatively little H -dependence until the excitation disappears at the edge of the Brillouin zone. These fits are used to calculate the magnetic dispersion in **(e)** along these two directions. A clear anisotropy appears about the BZ edge (dashed line). The inset shows a Q map of the data slices. Error bars correspond to an uncertainty of one standard deviation.

approach the BZ center Γ . Although the Q values of the excitations are incommensurate with respect to the reciprocal lattice vectors of the paramagnetic structure, the excitations do coincide with the BZ edges, so the typical use of the term commensurate may be confusing in this context.

Another outstanding feature is the width in E of the excitations in UTe_2 , which is comparable to the peak excitation energy, even at Q values where the excitations are sharpest. Despite these large widths, which imply substantially shortened excitation lifetimes or a distribution of transitions, the excitations are clearly peaked at nonzero E - therefore, these are inelastic features that are separated from the ground state by a finite energy gap. The peak energy of 4 meV matches well the hybridization gap determined in scanning tunneling spectroscopy measurements⁵, suggesting a connection to the electronic structure.

Signatures of hybridization

The temperature dependence of the excitations at $K = 1.4$ is shown in Fig. 3. Cooling below 5 K into the superconducting state yields an excitation spectrum that appears to remain mostly the same. In contrast, on warming from 5 to 20 K, the intensity decreases and the peak position increases slightly, but the

excitations maintain their Q -dependence and energy gap. Importantly, they do not move to lower E and become quasielastic, as might occur to magnetic correlations at temperatures above a magnetic phase transition. However, by 60 K the excitations are not discernable over the background. This temperature trend follows closely the low-field magnetic susceptibility along the crystallographic b -axis, whose peak at 40 K is a signature of the low-temperature development of the renormalized heavy fermion or hybridized electron state in UTe_2 . Multiple signatures of hybridization share a 4 meV energy scale: the temperature of the peak in the magnetic susceptibility¹, the temperature below which a sharp Drude peak develops in the optical conductivity¹², the hybridization gap determined from scanning tunneling spectroscopy⁵, and the magnetic gap measured by inelastic neutron scattering. One might then expect quasielastic neutron scattering at temperatures above the coherence temperature, but there is no observed movement of spectral weight to lower energy in the 20 K or 60 K data (Fig. 3). This may be related to the observation based on the optical conductivity that the formation of the heavy fermion state is associated primarily with a reduction in scattering rate, rather than redistribution of optical spectral weight¹².

Very similar inelastic BZ edge magnetic excitations are seen in the paramagnetic state in the heavy fermion superconductor

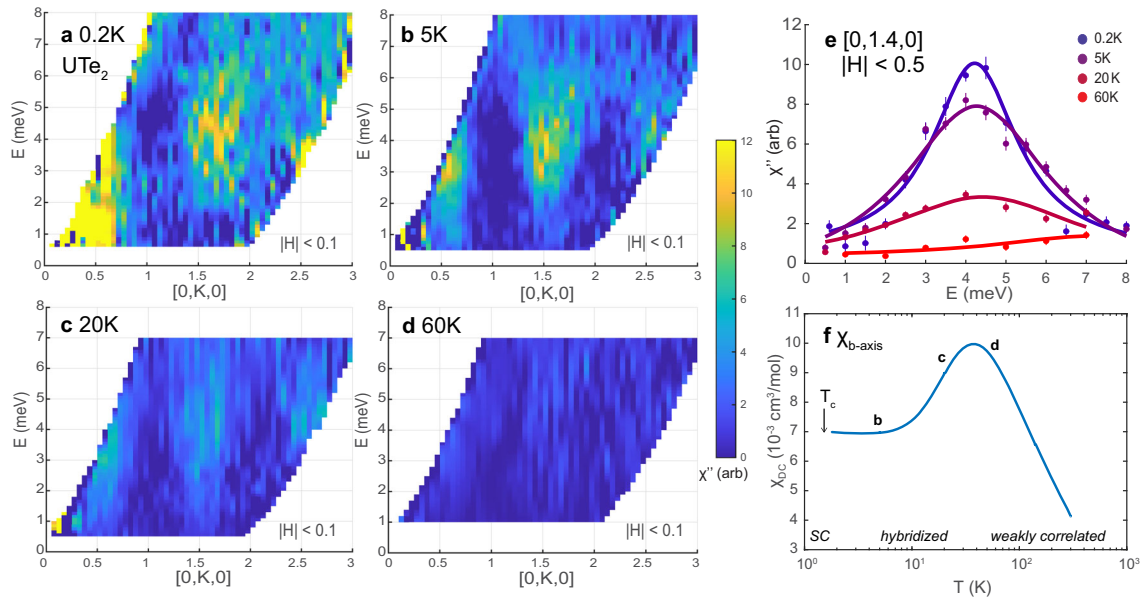


Fig. 3 Temperature dependence of the magnetic susceptibility in UTe_2 . $\chi''(Q, E)$ as a function of K at the BZ edge at (a) 0.2 K in the superconducting state, at (b) 5 K in the strongly hybridized, renormalized Fermi liquid state, at (c) 20 K where hybridization is weaker, and (d) at 60 K where correlations between local f electrons and light bands are weakest. **e** As temperature increases, the total spectral weight decreases but the magnetic susceptibility remains peaked at the same q value until it is no longer detectable above background. **f** This behavior follows closely the temperature-dependence of the bulk magnetic susceptibility χ along the b -axis (K direction)¹, which shows a hump structure characteristic of heavy fermion Kondo lattices ($1 \text{ cm}^3 \text{ mol}^{-1} = 4\pi \times 10^{-6} \text{ m}^3 \text{ mol}^{-1}$). The letters indicate the temperatures of the corresponding neutron data. Error bars correspond to an uncertainty of one standard deviation.

URu_2Si_2 ²⁴. There, the energy scale of the excitations is comparable to those in UTe_2 , and the anisotropy of the dispersion is analogous: the slopes are shallower along the BZ edge and steeper perpendicular to the edge. Both uranium compounds exhibit heavy fermion behavior, reflected in peaks in the electrical resistivity and magnetic susceptibility as a function of temperature, large Sommerfeld coefficients, and comparable spectroscopic gaps, signifying similar hybridization energy scales. Although the magnetic excitations in URu_2Si_2 fall at incommensurate Q vectors, they arise from interband scattering²⁵, as has been observed in other Kondo lattice compounds²⁶. A key geometric difference is that although both materials have body-centered crystal structures, URu_2Si_2 is tetragonal and its magnetic excitations follow the square BZ edges, while lines of excitations along only one rectangular edge are observed in orthorhombic UTe_2 . Therefore, anisotropy plays a central role in hybridization, and accurately determining the electronic structure is vital²⁷. In URu_2Si_2 , the onset of long-range hidden order opens a gap in the BZ edge excitations, but does not change their Q -dependence, because the long-range order maintains the heavy fermion state. Most importantly, the BZ edge excitations are remarkably robust, and even in chemically-tuned URu_2Si_2 , they persist regardless of whether the ordered state is hidden order²⁴, antiferromagnetism²⁸, or ferromagnetism²⁹. Consistent with this interpretation, UTe_2 lacks the additional zone-face excitations associated with hidden order and antiferromagnetism in URu_2Si_2 .

Therefore, the presence of incommensurate excitations in UTe_2 is insufficient to draw conclusions about incipient static magnetic order. Calculations do not provide strong constraints, as the dominant magnetic interactions in UTe_2 are easily tuned from ferromagnetic to antiferromagnetic³⁰. Many experiments suggest ferromagnetic interactions: muon spin relaxation¹⁵ and optical Kerr rotation experiments^{6,17} are consistent with low-temperature ferromagnetic correlations. As noted previously^{18,19} the absence of clear neutron scattering intensity near BZ centers as is seen in UCoGe ³¹ suggests that any magnetic fluctuations in UTe_2 that might be associated with an incipient order parameter or

quantum criticality are weak, but this is consistent with the bulk magnetization.

To account for this hybridization, it will be necessary to carry out further electronic structure and magnetic susceptibility calculations with higher energy resolution. Available calculations suggest that the strongest atomic exchange interaction in UTe_2 is ferromagnetic, between uranium dimers, with antiferromagnetic correlations parallel to the chains along the a -axis^{13,32}, but this does not readily explain the measured $\chi''(Q, E)$. The observed b -axis modulation has been considered to arise from the electronic structure, either Fermi surface nesting or RKKY exchange¹⁸. However, calculations to date have not yet addressed an important experimental point, namely that the measured $\chi''(Q, E)$ is peaked at small but finite energy, not at zero energy, the latter condition relevant to static magnetic order. Generally, given that these excitations appear to follow the temperature dependence of the b -axis bulk magnetic susceptibility, we expect that they will be quite robust as a function of magnetic field and could play a role in the magnetic transition at 35 T, and by extension, in the magnetically ordered phase above 1.5 GPa^{33–35}.

Superconducting state

The situation at lowest temperatures, in the superconducting state, brings an interesting twist. As Fig. 3 shows, the magnetic excitation spectrum is similar at 0.2 K and 5 K. Indeed, a significant difference is not expected at these energies, given the 1.6 K critical temperature and 0.25 meV gap observed in STM⁵. Therefore, the recently reported feature at 1 meV in the superconducting state^{20,21} suggests either a very large energy excitation of the superconducting state, or a modification of the established low-energy spin-fluctuations. In our measurements, it is not possible to conclusively identify the 1 meV feature at $K = 0.6$ because of the high background in that Q range, but it is not resolved at $K = 1.4$. Yet this feature is connected to the broader magnetic excitation and other changes in the magnetic spectrum are observed at 0.2 K. First, the dispersion along $[0, K, 0]$ is steeper for $K < 1.4$ and slightly gentler for $K > 1.4$ (Fig. 4a–d) than at 5 K. In fact, the

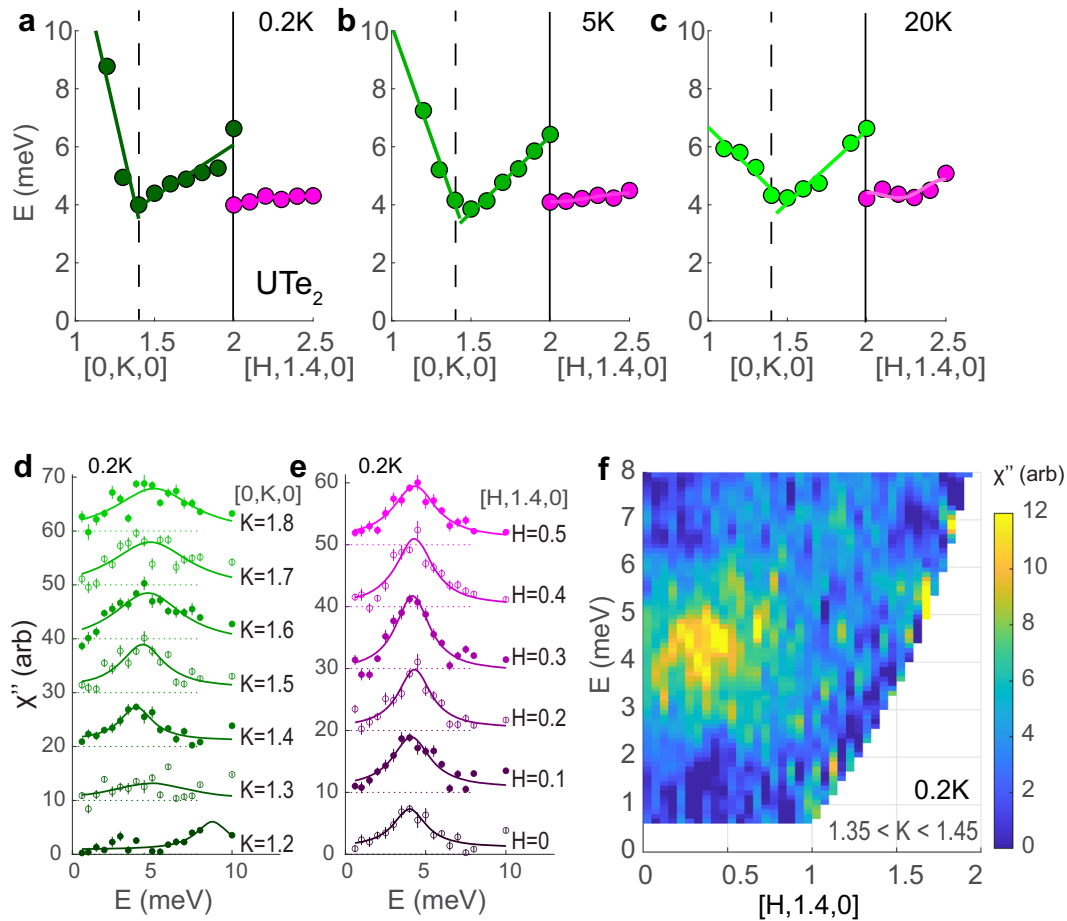


Fig. 4 Temperature dependence of the magnetic dispersion near the BZ edge at $[0, 1.4, 0]$. The lower- K dispersion is steeper in (a) the superconducting state, and gradually softens in (b) the normal state and at (c) higher temperatures. **d, e** Effective constant- Q scans show the E -dependence of χ'' at selected values of K from and H from (a). Note the relative intensity decreases at $[0, 1.4, 0]$ compared to 5 K (Fig. 2c). **f** $\chi''(Q, E)$ as a function of H at constant $K = 1.4$ in the superconducting state. Compare to Fig. 2b. Error bars correspond to an uncertainty of one standard deviation.

dispersion is weakly temperature-dependent at least to 20 K. Second, a slight decrease in intensity is observed near $[0, 1.4, 0]$ in the superconducting state (Fig. 4e, f), when compared to the data at 5 K (Fig. 2).

This behavior suggests that in the superconducting state, χ'' changes on energy scales even larger than 1 meV, and that previously reported feature reflects a larger change in the magnetic excitation spectrum. Such a broad change is difficult to reconcile with an interpretation in terms of a superconducting spin resonance. Since these magnetic excitations have their origin in the heavy fermion band structure, low-temperature changes in the electronic structure are likely responsible, and this is evidence that the superconducting state involves heavy quasiparticles. The change in the magnetic excitations may additionally correlate with low-temperature changes in the magnetic response in muon spin relaxation¹⁵ and nuclear magnetic resonance³⁶ inside the superconducting state.

In summary, inelastic neutron scattering measurements reveal magnetic excitations that are consistent with Kondo lattice phenomena. Specifically, the excitations follow BZ edges, obey the paramagnetic structural symmetry, and the temperature evolution of the heavy fermion bulk magnetic susceptibility along the b -axis. By analogy with other Kondo lattice compounds, these excitations are not directly related to an incipient magnetic ordered state. In the superconducting state, the magnetic

excitations near $[0, 1.4, 0]$ decrease in intensity, likely related to a change in the electronic structure.

METHODS

Sample synthesis

Single crystals of UTe_2 were synthesized by the chemical vapor transport method using iodine as the transport agent³⁷. The crystals are from synthesis batches that have been previously characterized^{1,3} and exhibit consistent properties.

Neutron experiment and analysis

Crystal orientation was determined by Laue x-ray diffraction performed with a Photonic Science x-ray measurement system. 1.2 g of single crystals, ranging in mass from 0.01 g to 0.1 g were coaligned and affixed to two copper plates using CYTOP fluoropolymer and Fomblin fluorinated grease. The crystalline mosaic is shown in Supplementary Fig. 1. Inelastic neutron scattering experiments were performed on the MACS spectrometer and preliminary measurements on the DCS spectrometer at the NIST Center for Neutron Research. Background subtraction and symmetrization are elaborated upon in Supplementary Methods.

DATA AVAILABILITY

The data that support the results presented in this paper and other findings of this study are available from the corresponding author upon reasonable request.

Received: 12 November 2021; Accepted: 23 February 2022;
Published online: 05 April 2022

REFERENCES

- Ran, S. et al. Nearly ferromagnetic spin-triplet superconductivity. *Science* **365**, 684–687 (2019).
- Aoki, D. et al. Unconventional superconductivity in heavy fermion UTe_2 . *J. Phys. Soc. Jpn.* **88**, 043702 (2019).
- Ran, S. et al. Extreme magnetic field-boosted superconductivity. *Nat. Phys.* **15**, 1250–1254 (2019).
- Knebel, G. et al. Field-reentrant superconductivity close to a metamagnetic transition in the heavy-fermion superconductor UTe_2 . *J. Phys. Soc. Jpn.* **88**, 063707 (2019).
- Jiao, L. et al. Chiral superconductivity in heavy-fermion metal UTe_2 . *Nature* **579**, 523–527 (2020).
- Hayes, I. M. et al. Multicomponent superconducting order parameter in UTe_2 . *Science* **373**, 797–801 (2021).
- Bae, S. et al. Anomalous normal fluid response in a chiral superconductor UTe_2 . *Nat. Commun.* **12**, 2644 (2021).
- Metz, T. et al. Point-node gap structure of the spin-triplet superconductor UTe_2 . *Phys. Rev. B* **100**, 220504 (2019).
- Ishihara, K. et al. Chiral superconductivity in UTe_2 probed by anisotropic low-energy excitations. Preprint at <http://arxiv.org/abs/2105.13721> (2021).
- Eo, Y. S. et al. Anomalous c-axis transport response of UTe_2 . Preprint at <http://arxiv.org/abs/2101.03102> (2021).
- Niu, Q. et al. Fermi-surface instability in the heavy-fermion superconductor UTe_2 . *Phys. Rev. Lett.* **124**, 086601 (2020).
- Mekonen, S. M. et al. An optical investigation of the heavy fermion normal state in superconducting UTe_2 . Preprint at <http://arxiv.org/abs/2105.05121> (2021).
- Miao, L. et al. Low energy band structure and symmetries of UTe_2 from angle-resolved photoemission spectroscopy. *Phys. Rev. Lett.* **124**, 076401 (2020).
- Hutanu, V. et al. Low-temperature crystal structure of the unconventional spin-triplet superconductor UTe_2 from single-crystal neutron diffraction. *Acta Crystallogr. B: Struct. Sci. Cryst. Eng. Mater.* **76**, 137–143 (2020).
- Sundar, S. et al. Coexistence of ferromagnetic fluctuations and superconductivity in the actinide superconductor UTe_2 . *Phys. Rev. B* **100**, 140502 (2019).
- Tokunaga, Y. et al. ^{125}Te -NMR study on a single crystal of heavy fermion superconductor UTe_2 . *J. Phys. Soc. Jpn.* **88**, 073701 (2019).
- Wei, D. S. et al. Interplay between magnetism and superconductivity in UTe_2 . *Phys. Rev. B* **105**, 024521 (2021).
- Duan, C. et al. Incommensurate spin fluctuations in the spin-triplet superconductor candidate UTe_2 . *Phys. Rev. Lett.* **125**, 237003 (2020).
- Knafo, W. et al. Low-dimensional antiferromagnetic fluctuations in the heavy-fermion paramagnetic ladder compound UTe_2 . *Phys. Rev. B* **104**, L100409 (2021).
- Duan, C. et al. Resonance from antiferromagnetic spin fluctuations for spin-triplet superconductivity in UTe_2 . *Nature* **600**, pages 636–640 (2021).
- Raymond, S. et al. Feedback of superconductivity on the magnetic excitation spectrum of UTe_2 . *J. Phys. Soc. Jpn.* **90**, 113706 (2021).
- Kreisel, A., Quan, Y. & Hirschfeld, P. J. Spin triplet superconductivity driven by finite momentum spin fluctuations. *Phys. Rev. B* **105**, 104507 (2022).
- Zic, M. P. et al. Coupled spin waves and crystalline electric field levels in candidate multiferroic $ErFeO_3$. *J. Appl. Phys.* **130**, 014102 (2021).
- Butch, N. P. et al. Symmetry and correlations underlying hidden order in URu_2Si_2 . *Phys. Rev. B* **91**, 035128 (2015).
- Brandow, B. H. Finite-temperature behavior of the Anderson lattice. *Phys. Rev. B* **37**, 250–260 (1988).
- Goremychkin, E. A. et al. Coherent band excitations in $CePd_3$: A comparison of neutron scattering and ab initio theory. *Science* **359**, 186–191 (2018).
- Denlinger, J. D. et al. Global perspectives of the bulk electronic structure of URu_2Si_2 from angle-resolved photoemission. *Electron. Struct.* **4**, 013001 (2022).
- Butch, N. P. et al. Distinct magnetic spectra in the hidden order and antiferromagnetic phases in $URu_{2-x}Fe_xSi_2$. *Phys. Rev. B* **94**, 201102 (2016).
- Butch, N. P., Rodriguez-Rivera, J. A. & Maple, M. B. Ungapped magnetic excitations beyond Hidden Order in $URu_{2-x}Re_xSi_2$. *Philos. Mag.* **100**, 1282–1288 (2020).
- Ishizuka, J. & Yanase, Y. Periodic Anderson model for magnetism and superconductivity in UTe_2 . *Phys. Rev. B* **103**, 094504 (2021).
- Stock, C. et al. Anisotropic critical magnetic fluctuations in the ferromagnetic superconductor $UCoGe$. *Phys. Rev. Lett.* **107**, 187202 (2011).
- Shishidou, T. et al. Topological band and superconductivity in UTe_2 . *Phys. Rev. B* **103**, 104504 (2021).
- Lin, W.-C. et al. Tuning magnetic confinement of spin-triplet superconductivity. *npj Quantum Mater.* **5**, 1–6 (2020).
- Ran, S. et al. Expansion of the high field-boosted superconductivity in UTe_2 under pressure. *npj Quantum Mater.* **6**, 1–5 (2021).
- Vališka, M. et al. Magnetic reshuffling and feedback on superconductivity in UTe_2 under pressure. *Phys. Rev. B* **104**, 214507 (2021).
- Nakamine, G. et al. Superconducting properties of heavy fermion UTe_2 revealed by ^{125}Te -nuclear magnetic resonance. *J. Phys. Soc. Jpn.* **88**, 113703 (2019).
- Ran, S. et al. Comparison of two different synthesis methods of single crystals of superconducting uranium ditelluride. *J. Vis. Exp.* **173**, e62563 (2021).

ACKNOWLEDGEMENTS

We thank Gabi Kotliar and Daniel Agterberg for helpful discussions and Yegor Vekhov for experimental assistance. Access to MACS and support for PMN and MPZ were provided by the Center for High Resolution Neutron Scattering, a partnership between the National Institute of Standards and Technology and the National Science Foundation under Agreement No. DMR-2010792. Research at the University of Maryland was supported by the National Institute of Standards and Technology, the Department of Energy Award No. DE-SC-0019154 (sample characterization) and the Gordon and Betty Moore Foundation's EPIQS Initiative through Grant No. GBMF9071 (materials synthesis). Identification of commercial equipment does not imply recommendation or endorsement by NIST.

AUTHOR CONTRIBUTIONS

N.P.B. conceived and designed the study. S.R. and S.R.S. synthesized the single crystals. S.R., S.R.S., P.M.N., and M.P.Z. coaligned the crystals. N.P.B., P.M.N., M.P.Z., S.G., Q.Y., and J.A.R. performed the neutron scattering measurements. N.P.B. analyzed the data and wrote the manuscript, with contributions from all authors.

COMPETING INTERESTS

The authors declare no competing interests.

ADDITIONAL INFORMATION

Supplementary information The online version contains supplementary material available at <https://doi.org/10.1038/s41535-022-00445-7>.

Correspondence and requests for materials should be addressed to Nicholas P. Butch.

Reprints and permission information is available at <http://www.nature.com/reprints>

Publisher's note Springer Nature remains neutral with regard to jurisdictional claims in published maps and institutional affiliations.



Open Access This article is licensed under a Creative Commons Attribution 4.0 International License, which permits use, sharing, adaptation, distribution and reproduction in any medium or format, as long as you give appropriate credit to the original author(s) and the source, provide a link to the Creative Commons license, and indicate if changes were made. The images or other third party material in this article are included in the article's Creative Commons license, unless indicated otherwise in a credit line to the material. If material is not included in the article's Creative Commons license and your intended use is not permitted by statutory regulation or exceeds the permitted use, you will need to obtain permission directly from the copyright holder. To view a copy of this license, visit <http://creativecommons.org/licenses/by/4.0/>.

This is a U.S. government work and not under copyright protection in the U.S.; foreign copyright protection may apply 2022